ESTIMATION OF UAV POSITION WITH USE OF SMOOTHING ALGORITHMS

Piotr Kaniewski, Rafał Gil, Stanisław Konatowski

Military University of Technology, Institute of Radioelectronics, Gen. S. Kaliski 2, 00-908 Warsaw, Poland
(✉ *pkaniewski@wat.edu.pl*, +48 261 839 080, *rgil@wat.edu.pl*, *skonatowski@wat.edu.pl*)

Abstract

The paper presents methods of on-line and off-line estimation of UAV position on the basis of measurements from its integrated navigation system. The navigation system installed on board UAV contains an INS and a GNSS receiver. The UAV position, as well as its velocity and orientation are estimated with the use of smoothing algorithms. For off-line estimation, a fixed-interval smoothing algorithm has been applied. On-line estimation has been accomplished with the use of a fixed-lag smoothing algorithm. The paper includes chosen results of simulations demonstrating improvements of accuracy of UAV position estimation with the use of smoothing algorithms in comparison with the use of a Kalman filter.

Keywords: Unmanned Aerial Vehicle, Inertial Navigation System, Global Navigation Satellite System, Integrated Navigation System, Synthetic Aperture Radar, Kalman Filter, Smoothing Algorithm.

1. Introduction

Unmanned Aerial Vehicles (UAV) are becoming more and more popular in military and civilian applications. In military context, they are applied mainly in *Electronic Intelligence* (ELINT) and *Imagery Intelligence* (IMINT) [1], which includes radar terrain imaging with the use of *Synthetic Aperture Radar* (SAR) [2−4].

The autonomy of operation requires that the position, velocity and angular orientation of UAV are estimated on-line and used for appropriate execution of its mission. Such an estimation is usually accomplished in an on-board integrated navigation system, typically composed of an *Inertial Navigation System* (INS) [5, 6] and a *Global Navigation Satellite System* (GNSS) receiver [5, 7], with the use of some form of *Kalman Filter* (KF) [8−15].

In some applications, *e.g.* SAR imagery, requirements with respect to the accuracy of positioning are very high [3, 4, 16, 17]. On the other hand, short delays in image availability are often acceptable. Thus, in this group of applications, fixed-lag smoothing algorithms [18, 19], which provide delayed but more accurate estimates than Kalman filters, can be applied to on-line estimation of UAV position. There are also applications where UAV trajectory and parameters of flight can be reconstructed off-line, after mission, on the basis of logged navigation data. In such a case, the authors suggest using very accurate fixed-interval smoothing algorithms [10, 18].

The layout of the paper is as follows. Firstly, a state-space model of an integrated navigation system used on-board UAV is presented. It is assumed that the system is loosely integrated according to the compensation method with feed-forward correction [5, 19] and is composed of an INS and a GNSS receiver. Such an INS/GNSS system has been designed and produced within the scope of the WATSAR project, performed by the Military University of Technology, Warsaw, Poland, and a Polish private company WB Electronics S.A. [17, 20]. Subsequently, the fixed-interval and the fixed-lag smoothing algorithms are described. The paper includes also chosen results of simulations, demonstrating improvements of accuracy of UAV position

estimation with the use of smoothing algorithms in comparison with the one using a Kalman filter. Finally, a discussion of the results and conclusions are presented.

2. State-space model of INS/GNSS system

Implementation of a Kalman filter or a smoothing algorithm in an INS/GNSS system requires previous formulation of its state-space model [5, 7]. In the case of a loosely integrated system [9], designed in the WATSAR project [17, 20], the discrete state-space model is linear and it is given by a pair of equations [11, 13−15]:

$$\mathbf{x}(k+1) = \mathbf{\Phi}(k+1,k)\mathbf{x}(k) + \mathbf{w}(k), \tag{1}$$

$$\mathbf{z}(k+1) = \mathbf{H}(k+1)\mathbf{x}(k+1) + \mathbf{v}(k+1), \tag{2}$$

where: $\mathbf{x}$ – a state vector; $\mathbf{w}$ – a vector of discrete random process disturbances; $\mathbf{z}$ – a measurement vector; $\mathbf{v}$ – a vector of measurement errors; $\mathbf{\Phi}$ – a transition matrix; $\mathbf{H}$ – an observation matrix.

Equation (1) is called the dynamics model and for the designed INS/GNSS system it describes propagation in time of errors of a custom-built INS. These errors include position, velocity and orientation errors resulting from processing erroneous inertial data inside the INS. Detailed INS errors models can be very complicated and may contain even several tens of states [7]. Some of these states are observable only conditionally, *e.g.* during maneuvers of UAV, and only in high-quality navigation-grade inertial systems. As in the WATSAR project only a medium-quality, tactical-grade INS has been used, a simple 9-state model of INS errors has been applied [17], with 3 states for position errors, 3 states for velocity errors and 3 states for orientation errors with respect to various axes of the local reference horizontal system of coordinates NED (North-East-Down) [9].

The 9-state dynamics model is originally continuous and it is based on a set of 9 scalar first-order differential equations, describing the relationship between the states constituting the state vector $\mathbf{x}$ and their first derivatives [5, 7]:

$$\dot{\delta N} = \delta v_N, \tag{3}$$

$$\dot{\delta v}_N = -f_D \phi_E + f_E \phi_D + u_{vN}, \tag{4}$$

$$\dot{\phi}_E = -\frac{1}{R}\delta v_N + \omega_N \phi_D + u_{\phi E}, \tag{5}$$

$$\dot{\delta E} = \delta v_E, \tag{6}$$

$$\dot{\delta v}_E = f_D \phi_N - f_N \phi_D + u_{vE}, \tag{7}$$

$$\dot{\phi}_N = \frac{1}{R}\delta v_E - \omega_E \phi_D + u_{\phi N}, \tag{8}$$

$$\dot{\delta D} = \delta v_D, \tag{9}$$

$$\dot{\delta v}_D = \frac{2g}{R}\delta D + u_{vD}, \tag{10}$$

$$\dot{\phi}_D = u_{\phi D}, \tag{11}$$

where: δN, δE, δD – INS position errors along the North, East and Down axes; δv_N, δv_E, δv_D – INS velocity errors along the North, East and Down axes; ϕ_N, ϕ_E, ϕ_D – INS attitude errors around the North, East and Down axes; f_N, f_E, f_D – specific forces along the North, East and Down axes; ω_N, ω_E – components of the angular velocity around the North and East axes; g – gravity acceleration; R – the Earth's radius in the spherical model; u_{vN}, u_{vE}, u_{vD} – errors of INS accelerometers; $u_{\phi N}$, $u_{\phi E}$, $u_{\phi D}$ – errors of INS gyros.

Grouping the above set of scalar equations into a single equation, we obtain the following continuous dynamics model of the system:

$$
\frac{d}{dt}\underbrace{\begin{bmatrix} \delta N \\ \delta v_N \\ \phi_E \\ \delta E \\ \delta v_E \\ \phi_N \\ \delta D \\ \delta v_D \\ \phi_D \end{bmatrix}}_{\dot{\mathbf{x}}(t)} = \underbrace{\begin{bmatrix} 0 & 1 & 0 & 0 & 0 & 0 & 0 & 0 & 0 \\ 0 & 0 & -f_D & 0 & 0 & 0 & 0 & 0 & f_E \\ 0 & -1/R & 0 & 0 & 0 & 0 & 0 & 0 & \omega_N \\ 0 & 0 & 0 & 0 & 1 & 0 & 0 & 0 & 0 \\ 0 & 0 & 0 & 0 & 0 & f_D & 0 & 0 & -f_N \\ 0 & 0 & 0 & 0 & 1/R & 0 & 0 & 0 & -\omega_E \\ 0 & 0 & 0 & 0 & 0 & 0 & 0 & 1 & 0 \\ 0 & 0 & 0 & 0 & 0 & 0 & 2g/R & 0 & 0 \\ 0 & 0 & 0 & 0 & 0 & 0 & 0 & 0 & 0 \end{bmatrix}}_{\mathbf{F}(t)} \cdot \underbrace{\begin{bmatrix} \delta N \\ \delta v_N \\ \phi_E \\ \delta E \\ \delta v_E \\ \phi_N \\ \delta D \\ \delta v_D \\ \phi_D \end{bmatrix}}_{\mathbf{x}(t)} + \underbrace{\begin{bmatrix} 0 & 0 & 0 & 0 & 0 & 0 \\ 1 & 0 & 0 & 0 & 0 & 0 \\ 0 & 1 & 0 & 0 & 0 & 0 \\ 0 & 0 & 0 & 0 & 0 & 0 \\ 0 & 0 & 1 & 0 & 0 & 0 \\ 0 & 0 & 0 & 1 & 0 & 0 \\ 0 & 0 & 0 & 0 & 0 & 0 \\ 0 & 0 & 0 & 0 & 1 & 0 \\ 0 & 0 & 0 & 0 & 0 & 1 \end{bmatrix}}_{\mathbf{G}(t)} \cdot \underbrace{\begin{bmatrix} u_{vN} \\ u_{\phi E} \\ u_{vE} \\ u_{\phi N} \\ u_{vD} \\ u_{\phi D} \end{bmatrix}}_{\mathbf{u}(t)},
$$

(12)

where: $\mathbf{F}$ – a fundamental disturbances.

The algorithms of filtration and smoothing presented further on in this paper are discrete, thus they require formulation of a discrete version of the state-space model for a given sampling period T. Thus, the above continuous dynamics model must be transformed into its discrete counterpart with the use of known methods presented *e.g.* in [7, 9–11]. The obtained discrete dynamics model is as follows:

$$
\underbrace{\begin{bmatrix} \delta N(k+1) \\ \delta v_N(k+1) \\ \phi_E(k+1) \\ \delta E(k+1) \\ \delta v_E(k+1) \\ \phi_N(k+1) \\ \delta D(k+1) \\ \delta v_D(k+1) \\ \phi_D(k+1) \end{bmatrix}}_{\mathbf{x}(k+1)} = \underbrace{\begin{bmatrix} 1 & T & -\frac{f_D T^2}{2} & 0 & 0 & 0 & 0 & 0 & \frac{f_E T^2}{2} \\ 0 & 1+\frac{f_D T^2}{2R} & -f_D T & 0 & 0 & 0 & 0 & 0 & f_E T - \frac{f_D \omega_N T^2}{2} \\ 0 & -\frac{T}{R} & 1+\frac{f_D T^2}{2R} & 0 & 0 & 0 & 0 & 0 & -\frac{f_E T^2}{2R}+\omega_N T \\ 0 & 0 & 0 & 1 & T & \frac{f_D T^2}{2} & 0 & 0 & -\frac{f_N T^2}{2} \\ 0 & 0 & 0 & 0 & 1+\frac{f_D T^2}{2R} & f_D T & 0 & 0 & -f_N T - \frac{f_D \omega_E T^2}{2} \\ 0 & 0 & 0 & 0 & \frac{T}{R} & 1+\frac{f_D T^2}{2R} & 0 & 0 & -\frac{f_N T^2}{2R}-\omega_E T \\ 0 & 0 & 0 & 0 & 0 & 0 & 1+\frac{gT^2}{R} & 1 & 0 \\ 0 & 0 & 0 & 0 & 0 & 0 & 2\frac{gT}{R} & 1+\frac{gT^2}{R} & 0 \\ 0 & 0 & 0 & 0 & 0 & 0 & 0 & 0 & 1 \end{bmatrix}}_{\Phi(k+1,k)} \cdot \underbrace{\begin{bmatrix} \delta N(k) \\ \delta v_N(k) \\ \phi_E(k) \\ \delta E(k) \\ \delta v_E(k) \\ \phi_N(k) \\ \delta D(k) \\ \delta v_D(k) \\ \phi_D(k) \end{bmatrix}}_{\mathbf{x}(k)} + \underbrace{\begin{bmatrix} w_N(k) \\ w_{vN}(k) \\ w_{\phi E}(k) \\ w_E(k) \\ w_{vE}(k) \\ w_{\phi N}(k) \\ w_D(k) \\ w_{vD}(k) \\ w_{\phi D}(k) \end{bmatrix}}_{\mathbf{w}(k)}.
$$

(13)

The observation model of the system describes a relationship between the measurements contained in the vector **z** and the states contained in the vector **x**. In the designed INS/GNSS system the measurements are formed from differences between INS and GNSS position and velocity components, thus they are linearly related to chosen elements of the state vector. The observation model for the described system is given as follows:

$$
\underbrace{\begin{bmatrix} R\left[\varphi^{INS}(k)-\varphi^{GNSS}(k)\right] \\ v_N^{INS}(k)-v_N^{GNSS}(k) \\ R\cos\varphi\left[\lambda^{INS}(k)-\lambda^{GNSS}(k)\right] \\ v_E^{INS}(k)-v_E^{GNSS}(k) \\ h^{INS}(k)-h^{GNSS}(k) \\ v_D^{INS}(k)-v_D^{GNSS}(k) \end{bmatrix}}_{z(k)} = \underbrace{\begin{bmatrix} 1 & 0 & 0 & 0 & 0 & 0 & 0 & 0 & 0 \\ 0 & 1 & 0 & 0 & 0 & 0 & 0 & 0 & 0 \\ 0 & 0 & 0 & 1 & 0 & 0 & 0 & 0 & 0 \\ 0 & 0 & 0 & 0 & 1 & 0 & 0 & 0 & 0 \\ 0 & 0 & 0 & 0 & 0 & 0 & -1 & 0 & 0 \\ 0 & 0 & 0 & 0 & 0 & 0 & 0 & 1 & 0 \end{bmatrix}}_{H(k)} \underbrace{\begin{bmatrix} \delta N(k) \\ \delta v_N(k) \\ \phi_E(k) \\ \delta E(k) \\ \delta v_E(k) \\ \phi_N(k) \\ \delta D(k) \\ \delta v_D(k) \\ \phi_D(k) \end{bmatrix}}_{x(k)} + \underbrace{\begin{bmatrix} v_N(k) \\ v_{vN}(k) \\ v_E(k) \\ v_{vE}(k) \\ v_D(k) \\ v_{vD}(k) \end{bmatrix}}_{v(k)}, \quad (14)
$$

where: φ^{INS}, λ^{INS}, h^{INS} – INS position coordinates (latitude, longitude, altitude); φ^{GNSS}, λ^{GNSS}, h^{GNSS} – GNSS position coordinates; v_N^{INS}, v_E^{INS}, v_D^{INS} – INS velocity components; v_N^{GNSS}, v_E^{GNSS}, v_D^{GNSS} – GNSS velocity components; v_N, v_E, v_D, v_{vN}, v_{vE}, v_{vD} – GNSS measurement errors; φ – the true latitude (in practice – approximated by the measured or estimated latitude).

To complete the model of the system it is necessary to calculate the covariance matrix **Q** of the vector **w** of discrete process disturbances and the covariance matrix **R** of the vector **v** of measurement errors. The matrix **Q** has been obtained with the use of the method presented in [9, 11] and is given below with (15) – (34):

$$
Q = \begin{bmatrix}
Q_{11} & Q_{12} & Q_{13} & -\dfrac{f_E f_N T^5}{20}S_{\varphi D} & -\dfrac{f_E f_N T^4}{8}S_{\varphi D} & Q_{16} & 0 & 0 & \dfrac{f_E T^3}{6}S_{\phi D} \\[2mm]
Q_{21} & Q_{22} & Q_{23} & -\dfrac{f_E f_N T^4}{8}S_{\varphi D} & -\dfrac{f_E f_N T^3}{3}S_{\varphi D} & Q_{26} & 0 & 0 & \dfrac{f_E T^2}{2}S_{\phi D} \\[2mm]
Q_{31} & Q_{32} & Q_{33} & Q_{34} & Q_{35} & Q_{36} & 0 & 0 & Q_{39} \\[2mm]
-\dfrac{f_E f_N T^5}{20}S_{\varphi D} & -\dfrac{f_E f_N T^4}{8}S_{\varphi D} & Q_{43} & Q_{44} & Q_{45} & Q_{46} & 0 & 0 & -\dfrac{f_N T^3}{6}S_{\phi D} \\[2mm]
-\dfrac{f_E f_N T^4}{8}S_{\varphi D} & -\dfrac{f_E f_N T^3}{3}S_{\varphi D} & Q_{53} & Q_{54} & Q_{55} & Q_{56} & 0 & 0 & -\dfrac{f_N T^2}{2}S_{\phi D} \\[2mm]
Q_{61} & Q_{62} & Q_{63} & Q_{64} & Q_{65} & Q_{66} & 0 & 0 & Q_{69} \\[2mm]
0 & 0 & 0 & 0 & 0 & 0 & \dfrac{T^3 S_{vD}}{3} & \dfrac{T^2 S_{vD}}{2} & 0 \\[2mm]
0 & 0 & 0 & 0 & 0 & 0 & \dfrac{T^2 S_{vD}}{2} & T S_{vD} & 0 \\[2mm]
\dfrac{f_E T^3}{6}S_{\varphi D} & \dfrac{f_E T^2}{2}S_{\varphi D} & Q_{93} & -\dfrac{f_N T^3}{6}S_{\varphi D} & -\dfrac{f_N T^2}{2}S_{\varphi D} & Q_{96} & 0 & 0 & T S_{\phi D}
\end{bmatrix}, \quad (15)
$$

$$
Q_{11} = \frac{T^3}{3}S_{vN} + \frac{f_D^2 T^5}{20}S_{\phi E} + \frac{f_E^2 T^5}{20}S_{\phi D}, \quad (16)
$$

$$
Q_{12} = Q_{21} = \frac{T^2}{2}S_{vN} + \frac{f_D^2 T^4}{8}S_{\phi E} + \frac{f_E^2 T^4}{8}S_{\phi D}, \quad (17)
$$

$$
Q_{13} = Q_{31} = -\frac{T^3}{3R}S_{vN} - \frac{f_D T^3}{6}S_{\phi E} + \frac{f_E \omega_N T^4}{8}S_{\phi D}, \quad (18)
$$

$$
Q_{22} = T S_{vN} + \frac{f_D^2 T^3}{3}S_{\phi E} + \frac{f_E^2 T^3}{3}S_{\phi D}, \quad (19)
$$

$$
Q_{23} = Q_{32} = -\frac{T^2}{2R}S_{vN} - \frac{f_D T^2}{2}S_{\phi E} + \frac{f_E \omega_N T^3}{3}S_{\phi D}, \quad (20)
$$

$$Q_{33} = \frac{T^3}{3R^2} S_{vN} + T S_{\phi E} + \frac{\omega_N^2 T^3}{3} S_{\phi D} \,, \tag{21}$$

$$Q_{16} = Q_{61} = -\frac{f_E \omega_E T^4}{8} S_{\phi D} - \frac{f_E f_N T^5}{20R} S_{\phi D} \,, \tag{22}$$

$$Q_{26} = Q_{62} = -\frac{f_E \omega_E T^3}{3} S_{\phi D} - \frac{f_E f_N T^4}{8R} S_{\phi D} \,, \tag{23}$$

$$Q_{34} = Q_{43} = -\frac{f_N \omega_N T^4}{8} S_{\phi D} + \frac{f_E f_N T^5}{20R} S_{\phi D} \,, \tag{24}$$

$$Q_{35} = Q_{53} = -\frac{f_N \omega_N T^3}{3} S_{\phi D} - \frac{f_E f_N T^4}{8R} S_{\phi D} \,, \tag{25}$$

$$Q_{36} = Q_{63} = -\frac{\omega_E \omega_N T^3}{3} S_{\phi D} + \frac{(f_E \omega_E - f_N \omega_N) T^4}{8R} S_{\phi D} + \frac{f_E f_N T^5}{20R^2} S_{\phi D} \,, \tag{26}$$

$$Q_{44} = \frac{T^3}{3} S_{vE} + \frac{f_D^2 T^5}{20} S_{\phi N} + \frac{f_N^2 T^5}{20} S_{\phi D} \,, \tag{27}$$

$$Q_{45} = Q_{54} = \frac{T^2}{2} S_{vE} + \frac{f_D^2 T^4}{8} S_{\phi N} + \frac{f_N^2 T^4}{8} S_{\phi D} \,, \tag{28}$$

$$Q_{46} = Q_{64} = \frac{T^3}{3R} S_{vE} + \frac{f_D T^3}{6} S_{\phi N} + \frac{f_N \omega_E T^4}{8} S_{\phi D} \,, \tag{29}$$

$$Q_{55} = T S_{vE} + \frac{f_D^2 T^3}{3} S_{\phi N} + \frac{f_N^2 T^3}{3} S_{\phi D} \,, \tag{30}$$

$$Q_{56} = Q_{65} = \frac{T^2}{2R} S_{vE} + \frac{f_D T^2}{2} S_{\phi N} + \frac{f_N \omega_E T^3}{3} S_{\phi D} \,, \tag{31}$$

$$Q_{66} = \frac{T^3}{3R^2} S_{vE} + T S_{\phi N} + \frac{\omega_E^2 T^3}{3} S_{\phi D} \,, \tag{32}$$

$$Q_{39} = Q_{93} = \frac{\omega_N T^2}{2} S_{\phi D} - \frac{f_E T^3}{6R} S_{\phi D} \,, \tag{33}$$

$$Q_{69} = Q_{96} = -\frac{\omega_E T^2}{2} S_{\phi D} - \frac{f_N T^3}{6R} S_{\phi D} \,, \tag{34}$$

where: $S_{vN}, S_{\phi E}, S_{vE}, S_{\phi N}, S_{vD}, S_{\phi D}$ – power spectral densities of Gaussian white noise in the vector **u** of continuous random process disturbances.

The measurement errors of GNSS receiver have been for simplicity modelled as uncorrelated in time and between each other Gaussian random sequences of zero mean and constant variance. As a result, the covariance matrix of measurement errors **R** is diagonal and is given as follows:

$$\mathbf{R} = \begin{bmatrix} \sigma_N^2 & 0 & 0 & 0 & 0 & 0 \\ 0 & \sigma_{vN}^2 & 0 & 0 & 0 & 0 \\ 0 & 0 & \sigma_E^2 & 0 & 0 & 0 \\ 0 & 0 & 0 & \sigma_{vE}^2 & 0 & 0 \\ 0 & 0 & 0 & 0 & \sigma_D^2 & 0 \\ 0 & 0 & 0 & 0 & 0 & \sigma_{vD}^2 \end{bmatrix}, \tag{35}$$

where: σ_N^2, σ_E^2, σ_D^2 – variances of position errors of the GNSS receiver; σ_{vN}^2, σ_{vE}^2, σ_{vD}^2 – variances of velocity errors of the GNSS receiver.

3. Kalman filtering algorithm

In applications requiring on-line estimation of the state-vector $\mathbf{x}(k)$ without delays, various filtering algorithms of the incoming navigation measurements are usually applied. The problem of filtering consists in finding state estimates of $\mathbf{x}(k)$ for all time steps k on the basis of all measurements made up to this time. Such an estimate is given as follows:

$$\hat{\mathbf{x}}(k \mid k) = E[\mathbf{x}(k) \mid \mathbf{z}(1), \dots, \mathbf{z}(k)]. \tag{36}$$

For linear systems, the optimal filtering algorithm is the linear Kalman filter [5, 9, 19]. Due to the linearity of the formulated model of the INS/GNSS integrated navigation system, the linear Kalman filter has been chosen as one of the algorithms to be designed and implemented in the system. A block diagram of the algorithm is presented in Fig. 1. It contains the initialization (step 1), executed once at the beginning of filter's operation, and recursively executed steps of time update (step 2), acquiring a new measurement (step 3) and a measurement update (step 4).
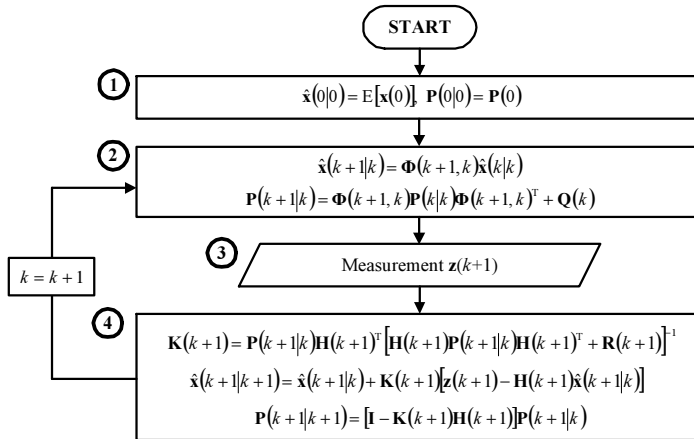

Fig. 1. The Kalman filtering algorithm.

The symbols used in the above diagram are as follows: $\hat{\mathbf{x}}(k+1 \mid k)$ – a predicted state vector in the time step $k + 1$; $\hat{\mathbf{x}}(k+1 \mid k+1)$ – corrected state vector in the time step $k + 1$; $\mathbf{P}(k+1 \mid k)$ – a covariance matrix of prediction errors; $\mathbf{P}(k+1 \mid k+1)$ – a covariance matrix of filtration errors; $\mathbf{K}(k+1)$ – a Kalman gains' matrix; $\mathbf{I}$ – an identity matrix. The other matrices used in the equations come from the previously defined state-space model of the system.

4. Smoothing algorithms

Apart from the above Kalman filter, two smoothing algorithms have been developed, *i.e.* a fixed-interval algorithm for off-line estimation and a fixed-lag algorithm for on-line estimation of position, velocity and orientation of UAV. The operation of smoothing consists in estimation of the state-space vector $\mathbf{x}(k)$ in the time step k on the basis of measurements from time steps later than k. Thus, it can be accomplished after mission of UAV or during its flight but with a short delay.

4.1. Fixed-interval smoothing algorithm

In the fixed-interval smoothing we assume that the measurements gathered in an interval $[0, N]$ are known. In our system they are registered on board UAV during flight. The algorithm is responsible for finding optimal state estimates of $\mathbf{x}(k)$ for all time steps k inside this interval on the basis of all known measurements. Such an estimate is given as follows:

$$\hat{\mathbf{x}}(k \mid N) = E[\mathbf{x}(k) \mid \mathbf{z}(1),\ldots,\mathbf{z}(N)], \tag{37}$$

for $k = 0,1, \ldots, N$. As the estimate is based on all available measurements, a properly executed fixed-interval smoothing provides the best possible estimate of the state vector.

There exist several methods of fixed-interval smoothing. One of the most commonly applied is an algorithm proposed by Rauch, Tung and Striebel [10, 19, 21, 22], known as the RTS algorithm. It is accomplished in two consecutive stages, *i.e.* forward and backward filtering. The forward filtering consists in calculation of estimates of the state vector $\mathbf{x}(k)$ with the use of the optimal KF. The results obtained in each time step k have to be registered for further use. It is necessary to store the estimates of the state vector obtained during filtration $\hat{\mathbf{x}}(k \mid k)$ and one-step prediction $\hat{\mathbf{x}}(k+1 \mid k)$ as well as their error covariance matrices $\mathbf{P}(k \mid k)$ and $\mathbf{P}(k+1 \mid k)$. In non-stationary systems, also variable values of the transition matrix $\mathbf{\Phi}(k+1,k)$ have to be stored. After this first stage of data processing, the backward filtering is accomplished with the initial conditions $\hat{\mathbf{x}}(N \mid N)$ and $\mathbf{P}(N \mid N)$, obtained as the final results of the forward filtering.

The optimal estimate of the state vector $\mathbf{x}(k)$ obtained during the fixed-interval smoothing is given as follows:

$$\hat{\mathbf{x}}(k \mid N) = \hat{\mathbf{x}}(k \mid k) + \mathbf{A}(k)[\hat{\mathbf{x}}(k+1 \mid N) - \hat{\mathbf{x}}(k+1 \mid k)], \tag{38}$$

where $\mathbf{A}(k)$ is the smoothing gain matrix:

$$\mathbf{A}(k) = \mathbf{P}(k \mid k)\mathbf{\Phi}^{\mathrm{T}}(k+1,k)\mathbf{P}^{-1}(k+1 \mid k) \quad \text{for } k = N-1, N-2, \ldots, 0. \tag{39}$$

The error covariance matrix of the fixed-interval smoothing is as follows:

$$\mathbf{P}(k \mid N) = \mathbf{P}(k \mid k) + \mathbf{A}(k)[\mathbf{P}(k+1 \mid N) - \mathbf{P}(k+1 \mid k)]\mathbf{A}^{\mathrm{T}}(k), \tag{40}$$

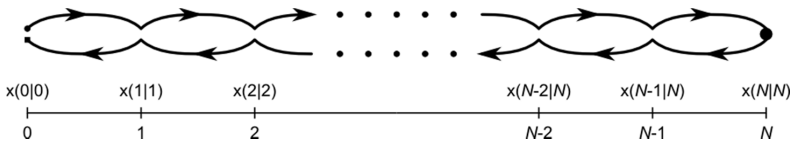for $k = N - 1, N - 2, \ldots, 0$. The idea of fixed-interval smoothing is explained in Fig. 2.

Fig. 2. The idea of fixed-interval smoothing.

The RTS algorithm is easy to implement but its drawback is a necessity of time-consuming inversions of the covariance matrix of prediction errors in (39). Other, less time-consuming fixed-interval smoothing algorithms can be found in literature [19, 23].

4.2. Fixed-lag smoothing algorithm

The fixed-lag smoothing algorithm processes incoming measurements on-line and calculates estimates of the state vector $\mathbf{x}(k)$ for time steps k delayed by a constant number of N steps in comparison with the current measurement. Such an estimate is given as follows:

$$\hat{\mathbf{x}}(k \mid k + N) = E[\mathbf{x}(k) \mid \mathbf{z}(1), \ldots, \mathbf{z}(k), \mathbf{z}(k+1), \ldots, \mathbf{z}(k+N)], \tag{41}$$

for $k = 0, 1, 2, \ldots$. The results of fixed-lag smoothing are less accurate than those of fixed-interval smoothing, since its estimates are based on a smaller amount of data. However, for large values of N, the accuracy of fixed-lag smoothing approaches the accuracy of the fixed-interval one, which will be demonstrated further on. Moreover, a possibility of using this algorithm on-line, during the flight of UAV, may be an important advantage in many applications.

The optimal estimates of the state vector in the fixed-lag smoothing are formed with the use of the following equation [10, 19]:

$$\hat{\mathbf{x}}(k+1-i \mid k+1) = \hat{\mathbf{x}}(k+1-i \mid k) + \mathbf{K}_i(k+1)\tilde{\mathbf{z}}(k+1), \tag{42}$$

for $i = 1, 2, \ldots, N$, where $\mathbf{K}_i(k+1)$ represents the gain matrix of the optimal fixed-lag smoother and it can be calculated as presented in [19]. The smoothing algorithm uses estimates of the state vector and residuals $\tilde{\mathbf{z}}(k+1)$ from a Kalman filter designed for the original state-space model. Thus, such a Kalman filter must be implemented to provide the data for the fixed-lag smoother. The smoothing algorithm can be accomplished in parallel to the Kalman filter.

As the estimate from the fixed-lag smoothing algorithm is delayed by N time steps, we can consider the smoothing process as accomplished in a time window of length N. This window is moving forward along the time scale as new measurements are processed. The idea of fixed-lag smoothing in a moving time window is explained in Fig. 3.
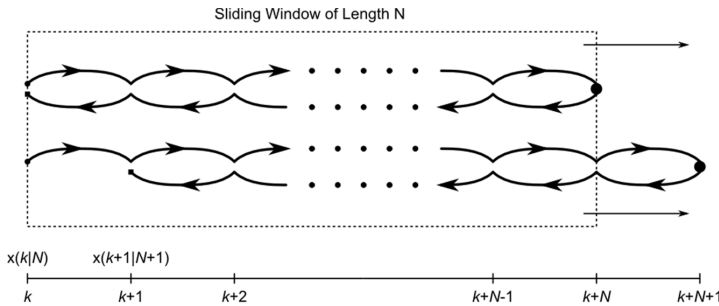

Fig. 3. The idea of fixed-lag smoothing.

The fixed-lag smoothing algorithm used in this paper is more complicated than the fixed-interval one as it requires numerous matrix multiplications in the process of calculation of the gain matrix of the optimal fixed-lag smoother $\mathbf{K}_i(k+1)$. If necessary, a simpler solution, where a fixed-interval smoothing is used to solve the fixed-lag smoothing problem can be found in the literature [18, 21].

5. Simulation results

The Kalman filter as well as both presented smoothing algorithms have been implemented in the assumed model of INS/GNSS system and simulated with the use of Matlab®. A Matlab toolbox called IRENA, developed at the Institute of Radioelectronics, at the Military University of Technology, Warsaw, Poland, have been used for this purpose [24]. The toolbox extends the Matlab functionality with useful functions enabling to simulate integrated navigation systems and their components.

During the simulations, a trajectory of flight of UAV, lasting 400 seconds, has been generated and used as a reference in testing filtering and smoothing algorithms. Then, INS and GNSS errors have been generated and added to the reference positions and velocities of UAV. For simplicity, the influence of internal Kalman filter, which is typically implemented in GNSS receivers, has been neglected and GNSS errors have been assumed to be Gaussian zero-mean, constant-variance white noise. Such an omission affects both filtering and smoothing, thus the comparisons of both types of algorithms do not affect their validity [25].

The parameters of INS and GNSS errors in the simulations have been chosen on the basis of technical specifications of real navigation devices used in the integrated system developed during the WATSAR project. These devices include an inertial 1750 IMU measurement unit from KVH Industries and a GNSS receiver built into an INS/GNSS(RTK) Ekinox-D system from SBG Systems. The values of the assumed parameters are given in Table 1.

Table 1. The values of parameters of INS and GNSS errors assumed in simulations.

Parameter	Value
$S_{\phi N}$, $S_{\phi E}$, $S_{\phi D}$	$1.15 \cdot 10^{-11}$ rad^2/s
S_{vN}, S_{vE}, S_{vD}	$1.4 \cdot 10^{-6}$ m^2/s^3
σ_N, σ_E, σ_D	1.2 m (SP), 0.4 m (DGNSS)
σ_{vN}, σ_{vE}, σ_{vD}	0.02 m/s

The parameters $S_{\phi N}$, $S_{\phi E}$, $S_{\phi D}$ represent power spectral densities of errors of gyros, whereas S_{vN}, S_{vE}, S_{vD} are power spectral densities of errors of accelerometers composing INS. The parameters σ_N, σ_E, σ_D represent standard deviations of GNSS position errors, and σ_{vN}, σ_{vE}, σ_{vD} are standard deviations of GNSS velocity errors expressed in the NED system of coordinates. The simulations have been performed for two different accuracy levels of GNSS possible in our system: the *standard positioning* (SP) accuracy and the accuracy of GNSS with differential corrections (DGNSS) [5]. A period of availability of new GNSS data has been assumed to be 0.5 second. The parameters given in Table 1 have also been used in implementation of the Kalman filter.

In the first step of simulations, the positioning errors of INS/GNSS system for SP and DGNSS levels of GNSS accuracy, with the Kalman filter and with the fixed-interval smoothing algorithm have been compared. These errors are expressed in the local horizontal NED reference system and their chosen results for the DGNSS level of accuracy are presented in Fig. 4–6.
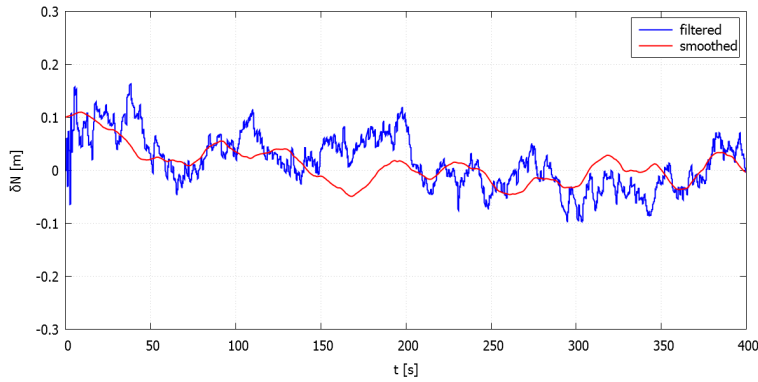
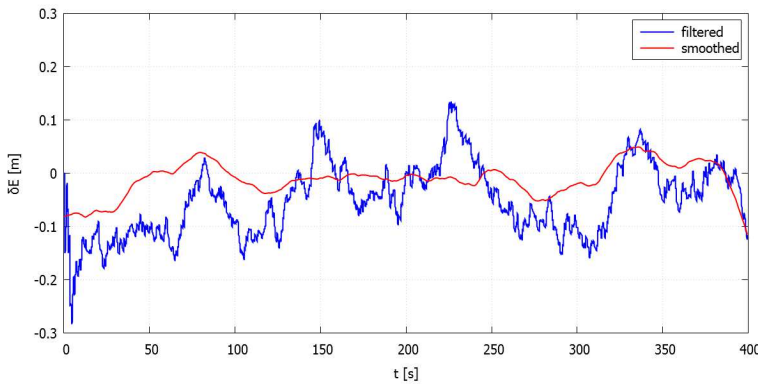Fig. 4. The positioning errors in INS/GNSS system in the north direction.

Fig. 5. The positioning errors in INS/GNSS system in the east direction.
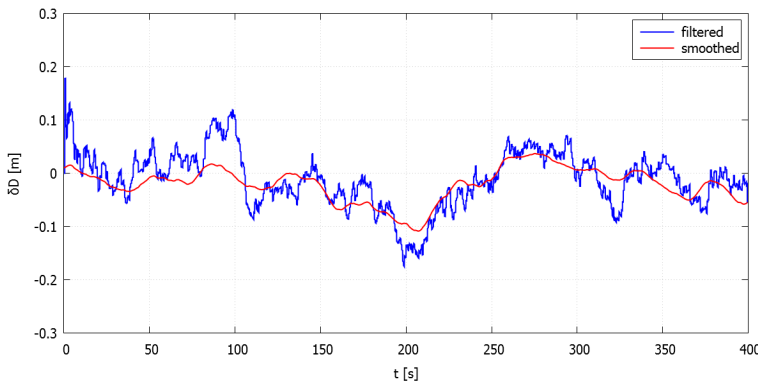

Fig. 6. The positioning errors in INS/GNSS system in the vertical (down) direction.

The above results show that the smoothed estimates of position are more accurate than the estimates from the Kalman filter. The level of improvement can be quantitatively assessed when we compare theoretical errors for various states estimated by both algorithms. The Kalman filter provides such information as its standard equations include a calculation of the error covariance matrix of filtration $\mathbf{P}(k \,|\, k)$ in each time step k. The smoothing algorithms do not include

or require such calculations, however, the error covariance matrix of smoothing can also be easily evaluated [9, 10, 19], which has been done for the purpose of comparisons. The diagonal elements of the error covariance matrices represent theoretical variances of estimation errors of respective states and their square roots are standard deviations of these errors. The comparison of theoretical standard deviations of positioning errors in the north direction for the entire period of simulations is shown in Fig. 7. Similar results have been obtained for other components of the state vector, therefore they are not included in the paper. From Fig. 7 we can see that, apart from the initial and final intervals of simulations, lasting 20 seconds each, the fixed-interval smoothing is about twice more accurate than the Kalman filter.
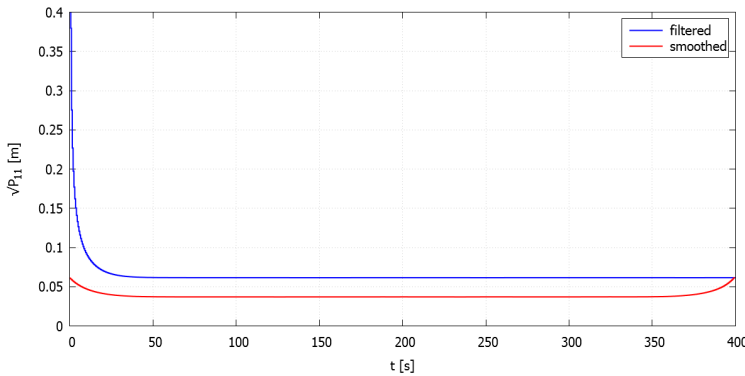

Fig. 7. The theoretical standard deviations of positioning errors in the north direction.

The comparison of filtering and fixed-interval smoothing accuracy can also be performed when calculating *root mean-squared* (RMS) errors of positioning for the whole period of simulation. The RMS errors of position for all axes of the NED reference system, as well as the total RMS positioning error calculated according to the following formula:

$$RMS(\delta_P) = \sqrt{[RMS(\delta_N)]^2 + [RMS(\delta_E)]^2 + [RMS(\delta_D)]^2} \qquad (43)$$

for SP and DGNSS levels of GNSS accuracy are presented in Table 2.

Table 2. The RMS errors of positioning in INS/GNSS system with a Kalman filter and a fixed-interval smoother.

Errors [m]	SP			DGNSS		
	Filtering	Smoothing	Reduction	Filtering	Smoothing	Reduction
$RMS(\delta_N)$	0.131	0.072	45.6%	0.067	0.038	43.6%
$RMS(\delta_E)$	0.134	0.073	45.4%	0.069	0.037	45.4%
$RMS(\delta_D)$	0.127	0.068	46.3%	0.065	0.036	45.0%
$RMS(\delta_P)$	0.226	0.123	45.8%	0.115	0.064	44.7%

The above results prove that the fixed-interval smoothing significantly reduces errors of position estimation in comparison with the Kalman filtering. Thus, for the assumed parameters of navigation devices, the off-line reconstruction of the UAV trajectory with the use of a fixed-interval smoother can be about twice as accurate as that with the use of a Kalman filter. This result is in accordance with the previously presented comparison of theoretical standard deviations of positioning errors (Fig. 7). The effects of error reduction are similar for all the coordinates and for both levels of GNSS accuracy.

In the next step of simulations, the positioning errors of INS/GNSS system for SP and DGNSS levels of GNSS accuracy, with a Kalman filter, fixed-interval and fixed-lag smoothing algorithms for various lags N have been compared. As a period between time steps in simulations is equal to 0.5 second, the time delay of the smoothed estimate is equal to $\Delta t = N/2$ seconds. The behavior of positioning errors follows a similar pattern for all the axes, therefore only the errors along the north axis, for the DGNSS level of accuracy, have been chosen for presentation and shown in Fig. 8−13.

The total RMS positioning errors for SP and DGNSS levels of GNSS accuracy for the Kalman filter, the fixed-interval smoother and the fixed-lag smoother with various delays are presented in Table 3. The error reduction in comparison with the filtering is shown in brackets. It is worth to notice that the relative level of error reduction asymptotically approaches a level equal to that of the fixed-interval smoother for both SP and DGNSS. However, when the correcting device (GNSS receiver) is more accurate, the progress of this reduction is quicker. Thus, the fixed-lag smoothing requires less delay to approach the quality of the fixed-interval one when a more accurate correcting sensor is used in the integrated navigation system.
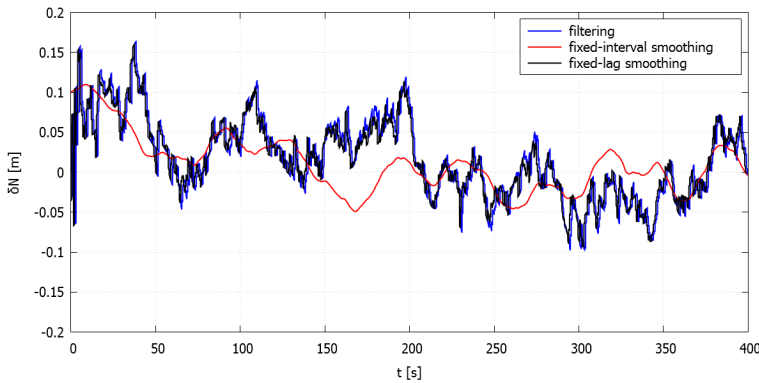

Fig. 8. The positioning errors in INS/GNSS system in the north direction
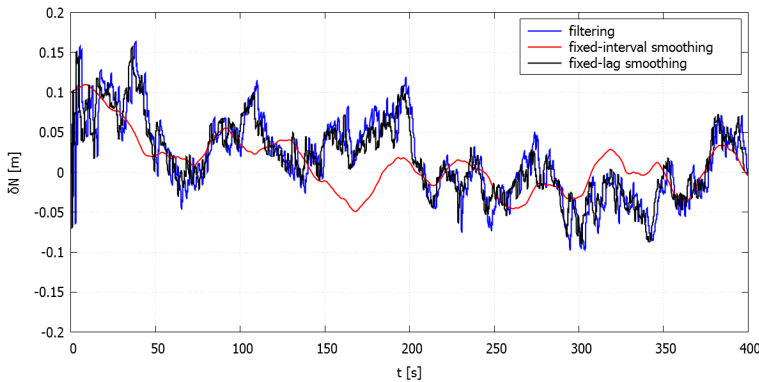($N = 1$, $\Delta t = 0.5$ s, in the fixed-lag smoothing).

Fig. 9. The positioning errors in INS/GNSS system in the north direction
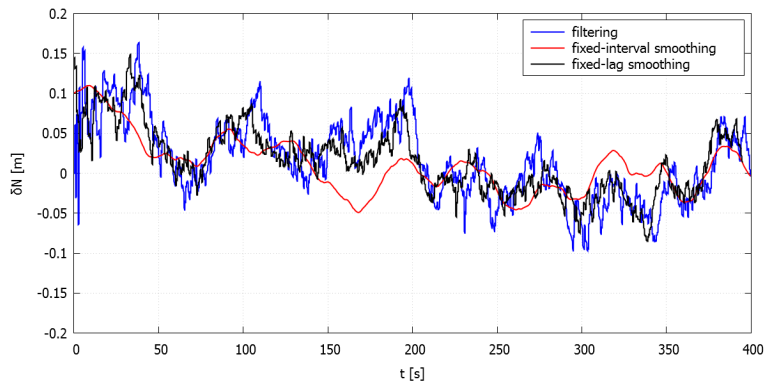($N = 2$, $\Delta t = 1$ s, in the fixed-lag smoothing).

Fig. 10. The positioning errors in INS/GNSS system in the north direction
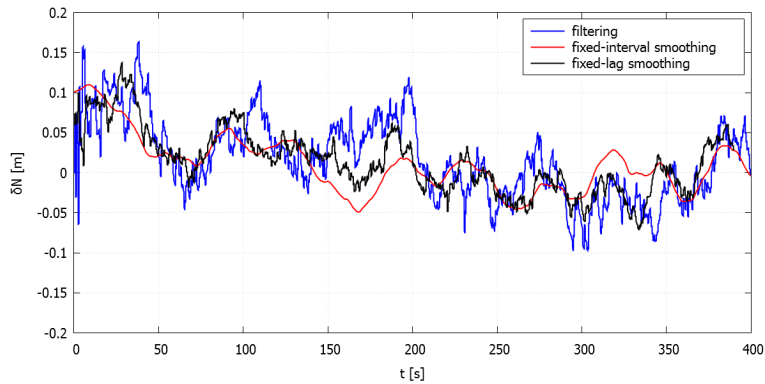($N = 5$, $\Delta t = 2.5$ s, in the fixed-lag smoothing).

Fig. 11. The positioning errors in INS/GNSS system in the north direction
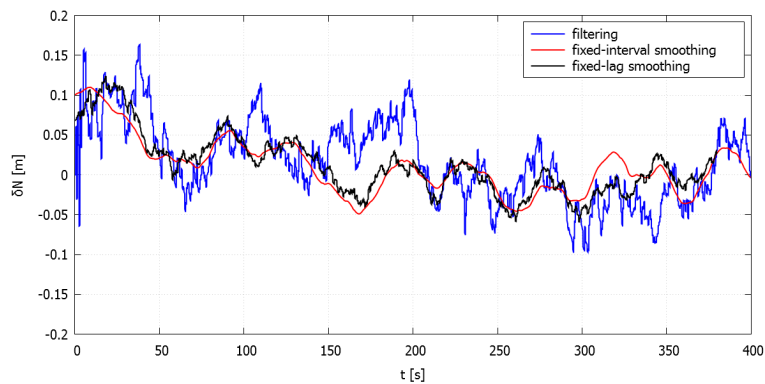$N = 10$, $\Delta t = 5$ s, in the fixed-lag smoothing).

Fig. 12. The positioning errors in INS/GNSS system in the north direction
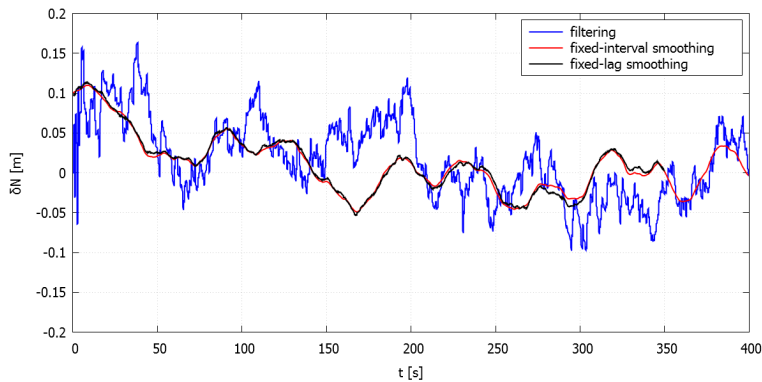($N = 20$, $\Delta t = 10$ s, in the fixed-lag smoothing).

Fig. 13. The positioning errors in INS/GNSS system in the north direction
($N = 50$, $\Delta t = 25$ s, in the fixed-lag smoothing).

Table 3. The RMS errors of positioning in INS/GNSS system with a Kalman filter and a fixed-lag smoother.

RMS(δ_P) [m]	Filtering	Fixed-lag smoothing for various delays						Fixed-interval smoothing
		$N = 1$	$N = 2$	$N = 5$	$N = 10$	$N = 20$	$N = 50$	
		$\Delta t = 0.5$s	$\Delta t = 1$s	$\Delta t = 2.5$s	$\Delta t = 5$s	$\Delta t = 10$s	$\Delta t = 25$s	
SP	0.226	0.217 (2.3%)	0.211 (5.4%)	0.197 (11.7%)	0.183 (18.2%)	0.164 (26.7%)	0.138 (39%)	0.123 (45.8%)
DGNSS	0.115	0.109 (4.8%)	0.104 (9.2%)	0.093 (18.2%)	0.083 (27.6%)	0.072 (37.5%)	0.064 (44.4%)	0.064 (44.7%)

6. Conclusions

The results presented in this paper demonstrate that both fixed-interval and fixed-lag smoothing algorithms can be very useful in specific navigation applications. A fixed-interval smoother can be used in post-processing of registered navigation data, *e.g.* for off-line reconstruction of the trajectory and parameters of flight of a UAV. In such an application, the accuracy of smoother is significantly better than the accuracy of a Kalman filter, which is typically used for this purpose. For the assumed parameters of devices, the errors of fixed-interval smoothing have been about twice smaller than the errors of filtering.

On the other hand, a fixed-lag smoother can be used instead of a Kalman filter for on-line estimation of position, velocity and orientation of a UAV, in applications accepting relatively small delay of the output data. Such applications include *e.g.* synthetic aperture radars which are an important type of image intelligence systems of today. The results presented in this paper demonstrate that a fixed-lag smoothing algorithm is more accurate than a Kalman filter. Its accuracy increases along with the increasing delay of estimates. Moreover, the accuracy of a fixed-lag smoother asymptotically approaches that of a fixed-interval one and makes it in a relatively short time. In the case of our system, it requires only several tens of seconds of delay, which can be acceptable in many applications.

It is important to notice that the use of a more accurate correcting device or a more accurate mode of its operation (*e.g.* DGNSS instead of SP in the case of a GNSS receiver) shortens the time necessary to achieve the required level of reduction of errors and a fixed-lag smoother can achieve the same level of accuracy with shorter delays.

Acknowledgements

References

[1] Matuszewski, J. (2008). Specific emitter identification. *International Radar Symposium*, Wroclaw, 1–4.

[2] Cumming, I.G., Wong, F.H., (2005). *Digital Processing of Synthetic Aperture Radar Data. Algorithms and Implementation*. Artech House.

[3] Mengdao, X., Xiuwei, J., Renbiao, W., Feng, Z., Zheng, B. (2009). Motion Compensation for UAV SAR Based on Raw Radar Data. *IEEE Transactions an Geoscience and Remote Sensing*, 8, 2870–2883.

[4] Samczyński, P., Malanowski, M., Gromek, D., Gromek, A., Kulpa, K., Krzonkalla, J., Mordzonek, M., Nowakowski, M. (2014). Effective SAR image creation using low cost INS/GPS. *International Radar Symposium*, Gdańsk, 174–177.

[5] Groves, P. (2008). *Principles of GNSS, Inertial, and Multisensor Integrated Navigation Systems*. Artech House.

[6] Titterton, D.H., Weston, J.L. (2004). Strapdown Inertial Navigation Technology. *Institution of Electrical Engineers*, UK, 17–57.

[7] Farrell, J.A. (2008). *Aided Navigation GPS with High Rate Sensors*. McGraw-Hill.

[8] Anderson, B.D.O., Moore, J.B. (1979). *Optimal Filtering*. Prentice-Hall, INC, Englewood Cliffs, New Jersey.

[9] Brown, R.G., Hwang, P.Y.C. (2012). *Introduction to Random Signals and Applied Kalman Filtering*. John Wiley & Sons, Inc.

[10] Särkkä, S. (2013). *Bayesian filtering and smoothing*. Cambridge University Press.

[11] Kaniewski, P. (2010). *Structures, models and algorithms in integrated positioning and navigation systems*. Wyd. WAT, Warszawa.

[12] Gelb, A. (2001). *Applied Optimal Estimation*. Massachusetts Institute of Technology, Cambridge, Massachusetts and London.

[13] Li, X., Xie, Y., Bi, D., Ao, Y. (2013). Kalman Filter Based Method for Fault Diagnostics of Analog Circuits. *Metrol. Meas. Syst.*, 20(2), 307–322.

[14] Konatowski, S., Pieniężny, A.T. (2007). A comparison of estimation accuracy by the use of KF, EKF & UKF filters. *WIT Transactions on Modelling and Simulation*, 46, 779–789.

[15] Śmieszek, M., Dobrzańska, M. (2015). Application of Kalman Filter in Navigation Process of Automated Guided Vehicles. *Metrol. Meas. Syst.*, 22(3), 443–454.

[16] Fornaro, G. (1999). Trajectory deviations in airborne SAR: analysis and compensation. *IEEE Transactions on Aerospace and Electronics Systems*, 35(3), 997–1009.

[17] Kaniewski, P., Leśnik, C., Susek, W., Serafin, P. (2015). Airborne radar terrain imaging system. *International Radar Symposium*, Dresden, 248–253.

[18] Einicke, G.A. (2012). *Smoothing, Filtering and Prediction: Estimating the Past, Present and Future*. Published by InTech.

[19] Meditch, J.S. (1969). *Stochastic Optimal Linear Estimation and Control*. New York, McGraw Hill.

[20] Łabowski, M., Kaniewski, P., Konatowski, S., (2016). Estimation of flight path deviations for SAR radar installed on UAV. *Metrol. Meas. Syst.*, 23(3), 383–391.

[21] Rauch, H.E., (1963). Solutions to the Linear Smoothing Problem. *IEEE Transactions on Automatic Control*, 8, 371–372.

[22] Rauch, H.E., Tung, F., Striebel, C.T. (1965). Maximum Likelihood Estimation of Linear Dynamic Systems. *AIAA Journal*, 3(8), 1445–1450.

[23] Techy, L., Morgansen, K.A., Woolsey, C.A. (2011). Long-baseline acoustic localization of the Seaglider underwater glider. *American Control Conference (ACC)*, San Francisco.

[24] Kaniewski, P., Konatowski, S., (2014). Software Toolbox for Simulation of Integrated Navigation Systems. *Przegląd Elektrotechniczny*, 90(8), 168–171.

[25] Bednarek, M., Będkowski, L. (2008). Dąbrowski T.: Comparative-threshold diagnosing in messages transmission system. *Przegląd Elektrotechniczny*, 84(11A), 320–324.